Korean J. Chem. Eng., 36(5), 753-762 (2019)
DOI: 10.1007/s11814-019-0261-7

pISSN: 0256-1115
eISSN: 1975-7220

Preparation of mesoporous silica from coal slag and its metal ion adsorption behavior

Xinying Zhang*, Yu Wu*,, Xuefang Li*,**, Xianlong Meng*,**, Huihu Shi*,**, Zhaojun Wu*,**, and Jianbin Zhang*,**,†**

*College of Chemical Engineering, Inner Mongolia University of Technology, Hohhot 010051, China
**Inner Mongolia Engineering Research Center for CO_2 Capture and Utilization, Hohhot 010051, China
(*Received 21 October 2018 • accepted 1 April 2019*)

Abstract−A novel mesoporous silica (MS) with the high specific surface area up to 1,199 m^2/g was prepared from coal slag by SO_3^{2-} leaching and hydrothermal synthesis. Its application in metal ion removal was explored using Pb^{2+}, Cu^{2+}, Co^{2+} and Cd^{2+} as the model ions. The effects of adsorption time, pH, initial metal ion concentration, adsorbent dosage and adsorption temperature on the metal ion adsorption behaviors of the as-prepared MS were systematically, and the maximum adsorption capacities were measured to be 55.76 $mg \cdot g^{-1}$, 33.49 $mg \cdot g^{-1}$, 24.29 $mg \cdot g^{-1}$ and 22.98 $mg \cdot g^{-1}$ for Pb^{2+}, Cu^{2+}, Co^{2+} and Cd^{2+}, respectively. The metal ion adsorption on the as-prepared MS followed pseudo-second-order kinetics, and the adsorption isotherm fitted the Langmuir isotherm model, indicating that the adsorption was spontaneous, endothermic and enthalpy driven.

Keywords: Mesoporous Silica, Coal Slag, Hydrothermal Synthesis, Metal Ion, Adsorption Behaviors

INTRODUCTION

Coal slag is one of the major industrial solid wastes in China because of high volumes of coal combustion [1,2]. The production of coal slag has increased by ~330 mt/y [3], which poses a great threat to the environment and agricultural industries [4-7]. In general, each ton of coal produces 0.25-0.3 t coal slag. The coal slag is mainly converted into construction materials, such as bricks, cement and so on, yet with the utilization rate of only 15% in China [8,9], this significantly limits its utilization efficiency. Therefore, improving the coal slag recycle by chemical conversion has drawn considerable attention, such as the extraction of Si, Al and Fe from coal slag [10-12].

Mesoporous silica (MS) possesses excellent properties, such as high surface areas, uniform channels, adjustable pore sizes and large pore volumes, and thus has exhibited great application potential as a mesoporous molecular sieve [13-15]. In addition, its unique chemical structure with silanol (Si-OH) functional group [16,17], uniform hexagonal array pore distribution and various elements within the silica framework endow its applicability as chemical sensors, reaction catalysts, catalysts supports and adsorbents [18-21]. So far, MS has been mainly synthesized with various pure silica precursors, such as silicon alkoxide, fumed silica, and soluble silicates [12], which significantly increases the production cost. Coal slag contains abundant silicon and can be a source material for the preparation of MS at low cost. To the best of our knowledge, the synthesis of MS from coal slag has been rarely explored, and the related work remains a great challenge.

Wastewaters produced from chemical manufacturing, electrical apparatus, and battery industries usually contain large amounts of metal ions, such as Pb^{2+}, Cd^{2+}, Cu^{2+}, Hg^{2+} and Zn^{2+}, which is highly hazardous to the ecosystem and human health. Metal ion removal is a major process in wastewater treatment. A variety of approaches have been developed for metal ion removal, such as ion exchange, chemical precipitation, membrane separation, reverse osmosis, and adsorption [22-25]. Compared to other approaches, adsorption shows unique advantages of low energy consumption and high removal efficiency. MS has been demonstrated as an excellent metal ion adsorbents with the better performances than activated carbon, zeolite, diatomite and clay [26,27].

In the present work, a green and simple approach to preparation of MS with coal slag by SiO_3^{2-} leaching and hydrothermal synthesis is reported. The as-prepared MS was systemically characterized by FTIR, N_2 adsorption-desorption, XRF, XRD, SEM, and TEM, and its application in the heavy metal ions removal from wastewater was explored. Our work has provided a novel strategy of coal slag utilization for metal ion remove.

EXPERIMENTAL

1. Materials

Coal slag was supplied from the Baotou third thermal power plant, China. Cetyltrimethylammonium bromide (CTAB, A.R., Sinopharm), sodium hydroxide (A.R., Sinopharm), $Pb(NO_3)_2$, $CuSO_4 \cdot 5H_2O$, $Co(NO_3)_2 \cdot 6H_2O$, $CdCl_2$, and HCl were all commercially available chemicals and used as-received without further purification. The chemical composition of coal slag was analyzed by XRF technology and shown in Table 1.

2. Preparation of SiO_3^{2-} Solution from Coal Slag

Coal slag was ground, passed through a 200 mesh sieve and dried at 120 °C for 12 h. Fifteen grams of dried coal slag was stirred in 100 mL 20 wt% HCl at 80 °C for 2 h to remove iron and oxides. The acid leached coal slag was then washed with distilled water until neutral, dried at 105 °C for 24 h, and cooled to room tem-

†To whom correspondence should be addressed.
E-mail: tadzhang@pku.edu.cn

Table 1. Chemical composition of the coal slag (%)

Composition	SiO_2	Al_2O_3	Fe_2O_3	CaO	MgO	SO_3	Others
Content (%)	47.56	40.05	2.85	2.55	0.90	0.63	5.46

perature for further use.

The acid leached coal slag with particle size of 80-400 mesh was mixed with 30 g NaOH in appropriate volumes of water with the final NaOH concentration of 5%-30%, and reacted at 70-100 °C for 30-240 min. The leaching liquid was filtered and combined with the wash solution of coal slag to give a SiO_3^{2-} solution.

3. Preparation of MS

In a typical procedure, 0.5 g CTAB was dissolved in 10 mL deionized water at 40 °C to form an aqueous micellar solution that was then mixed with the SiO_3^{2-} solution (pH=13-14) obtained above. The pH of the mixture was adjusted with 2.5 mol/L HCl until white precipitation was observed (pH=10). The mixture was then put into a hydrothermal synthesis reactor, reacted at 120 °C for 24 h and filtered. The residue was washed repeatedly with deionized water, dried at 105 °C for 12 h, and calcined at 550 °C for 6 h at the heating rate of 2 °C/min in air to afford MS.

4. Characterization

The chemical composition of coal slag was analyzed by the XRF spectrometer (Rigaku ZSX Primus II). FTIR measurement using KBr self-supported pellet technique was performed on Nicolet, Nexus 670, in the wavenumber range of (4,000 to 400) cm^{-1}. The MS patterns were determined by using a Shimadzu, D/max-2200/PC XRD. Radiation of Cu Kα was generated using an X-ray generator. The scanning range of 2θ was set at 2°-60° with a step of 2°/min. SEM analyses used a HITACHI, S-3400N. TEM analysis was performed using a JEM-2100F as well as the elemental analysis. The standard BET method was used to measure the specific surface area of the adsorbent on the basis of the physical adsorption of N_2 on the solid surface (Beishide, 3H-2000PS1/2 Specific surface & pore size analysis instrument).

5. Adsorption Kinetic Studies

The formulas for calculating the adsorption capacity (q_e) and removal rate (Removal) are as follows:

$$q_e = \frac{C_0 - C_e}{W} \cdot V \tag{1}$$

$$\text{Removal} = \frac{C_0 - C_e}{C_0} \times 100 \tag{2}$$

q_e-Adsorption capacity of adsorbent (mg/g)
C_0-Initial concentration of metal ion solution
C_e-Concentration of metal ion solution at equilibrium
V-Volume of solution
W-Quality of Adsorbent MS

5-1. Pseudo-first-order Kinetic Model

The model [28] was widely used in the adsorption processes, and the model was as follows:

$$\frac{dq}{dt} = k_1(q_e - q) \tag{3}$$

After integration:

$$\ln\frac{q_e - q_t}{q_e} = -kt \tag{4}$$

$$\ln(q_e - q_t) = \ln(q_e) - k_1 t \tag{5}$$

k_1-equilibrium rate constant, min^{-1}

5-2. Pseudo-second-order Kinetic Model [29]

The adsorption was controlled by a chemical mechanism. It was related to electronic transfer and electronic sharing between adsorbate and adsorbent.

$$\frac{dq}{dt} = k_2(q_e - q)^2 \tag{6}$$

After integration,

$$\frac{1}{q_e - q_t} = \frac{1}{q_e} + k_2 t \tag{7}$$

$$\frac{t}{q_t} = \frac{1}{k_2 q_e^2} + \frac{t}{q_e} \tag{8}$$

6. Adsorption Isotherms

6-1. Langmuir Adsorption Isotherm

Langmuir assumes that the adsorbent surface is uniform and there is no interaction among adsorbents. Adsorption is a monolayer adsorption process, namely adsorption occurs only on the external surface of the adsorbents. The equations are shown as follows [30,31]:

$$q_e = \frac{bq_m C_e}{1 + bC_e} \tag{9}$$

$$\frac{1}{q_e} = \frac{1}{bq_m C_e} + \frac{1}{q_m} \tag{10}$$

q_e-equilibrium adsorption capacity, $mg \cdot g^{-1}$
q_m-monolayer saturated adsorption capacity, $mg \cdot g^{-1}$
b-Langmuir equilibrium constant, $L \cdot mg^{-1}$
C_e-equilibrium concentration of metal ions, $mg \cdot L^{-1}$

6-2. Freundlich Adsorption Isotherm Model

Freundlich model can accurately describe the adsorption mechanism on a uniform surface. In a wider range of concentration, it can explain the experimental results very well. The equations are as follows [32,33]:

$$q_e = kC_e^{1/n} \tag{11}$$

$$\ln q_e = \ln k + \frac{1}{n}\ln C_e \tag{12}$$

k_f-Freundlich equilibrium constant, L/g
n-heterogeneity factor

7. Adsorption Thermodynamics

Adsorption thermodynamics is also important in describing the adsorption process. Thermodynamic parameters at different tem-

peratures are calculated using adsorption thermodynamics. The formulas are as follows:

$$K_e = \frac{q_e}{c_e} \tag{13}$$

$$\Delta G = -RT\ln K_e \tag{14}$$

$$\ln K_e = -\frac{\Delta H}{RT} + \frac{\Delta S}{R} \tag{15}$$

According to the experimental data, $\ln K_e$ and 1000/T are used to plot the vertical and horizontal coordinates, respectively. Gibbs's free energy (ΔG), entropy change (ΔS) and enthalpy change (ΔH) are calculated by the slope and intercept. If the ΔG<0, the adsorption behavior is spontaneous, Conversely, the adsorption behavior is not spontaneous. If ΔH<0, the adsorption process is exothermic reaction; on the contrary, the adsorption process is an endothermic process, and heating is favorable for adsorption. If ΔH> T·ΔS, the adsorption process is enthalpy driven. Otherwise, it is an entropy driven process.

RESULTS AND DISCUSSION

1. Preparation of Leaching Liquid from Coal Slag

The effects of particle size of coal slag on the SiO_3^{2-} leaching efficiency were investigated in 15% NaOH with the mass ratio of NaOH to coal slag of 2 : 1 and reaction time of 120 min. The results suggested the extraction efficiency of silica increased with the decrease of particle size (Fig. 1(a)). For example, the extraction efficiency increased from 57.45% to 65.20% as the particle size of coal slag decreased from 80 mesh to 200 mesh. It can be explained that smaller coal slag particles possess larger surface areas that are conducive to leaching, thus increasing the SiO_3^{2-} concentration and improving the porous properties. Further decreasing the particle size to 300-400 mesh slightly increased the extraction efficiency. However, extremely small particles became a challenge for filtration. Therefore, the particle size was optimized to be 200 mesh, which resulted in the SiO_3^{2-} extraction efficiency of 65.20%.

The leaching was then conducted in 5%, 10%, 15%, 20% and 25% NaOH, respectively, at the mass ratio of NaOH to coal slag of 2 : 1 with 200 mesh coal slag at 95 °C for 120 min to determine the optimal NaOH concentration. As shown in Fig. 1(b), the leaching efficiency increased with the increase of NaOH concentration and peaked at 15% due to the high collision probability between coal slag and NaOH. Further increasing NaOH concentration resulted in decreased extraction efficiency of silica because of extensive secondary reactions. Therefore, the NaOH concentration was optimized to be 15% and used in the following experiments unless stated otherwise.

The effect of reaction temperature on the extraction efficiency of silica was investigated in the range of from 70 °C to 100 °C at the mass ratio of NaOH to coal slag of 2 : 1 with 200 mesh coal slag and reaction time of 120 min. It was found that the extraction efficiency increased with the increase of reaction temperature and peaked at 95 °C with the value of 65.18%. It can be explained that higher reaction temperatures increased the chemical reaction rate and the liquid-solid collision probability. Therefore, the reaction was conducted at 95 °C in the following experiments.

The effects of reaction time in the range of 30-180 min on the extraction efficiency of silica were investigated at the mass ratio of NaOH to coal slag of 2 : 1 with 200 mesh coal slag. As shown in Fig. 1(d), the extraction efficiency gradually increased to 65.18% as the reaction time prolonged from 30 min to 120 min, and reached 65.30% at 180 min. For economic purposes, the reaction time was set to 120 min.

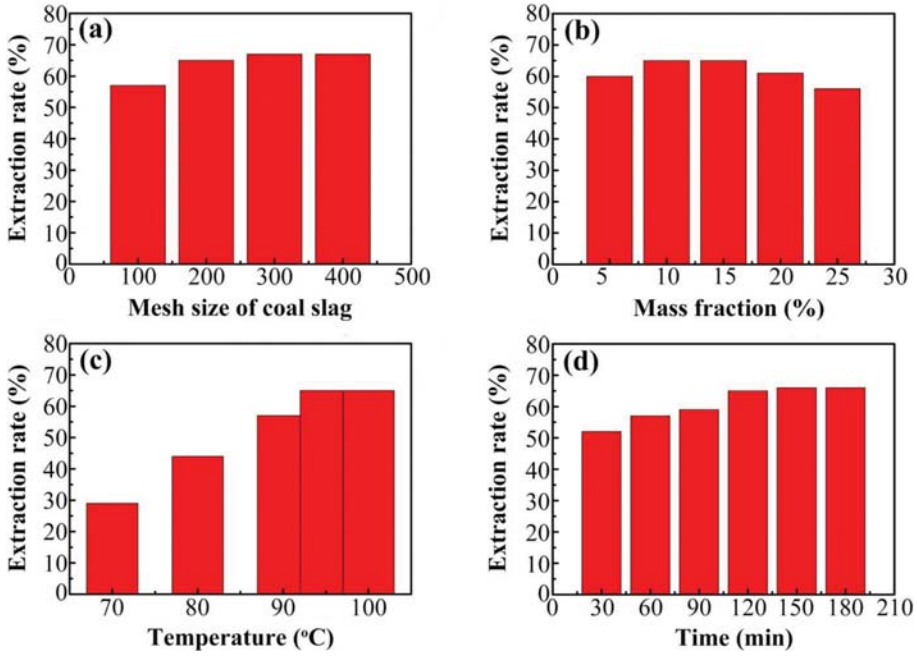

Fig. 1. (a) The effect of particle size, (b) alkali mass fraction, (c) reaction temperature and (d) reaction time on the extraction of silica.

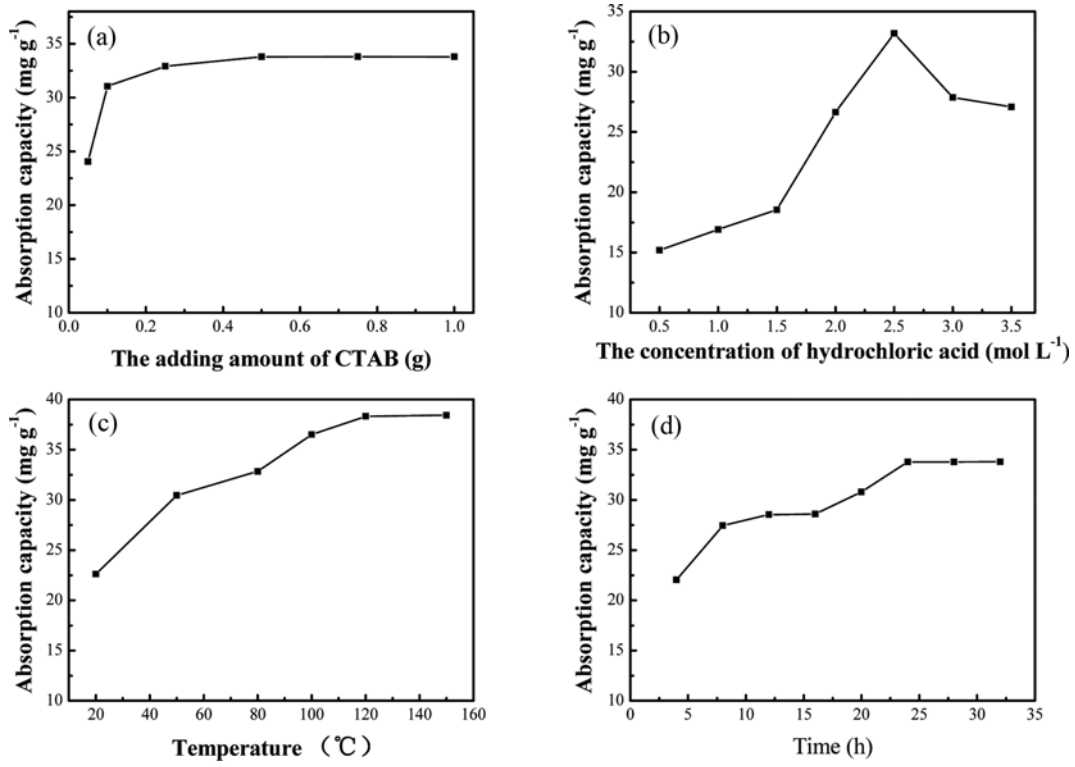

Fig. 2. (a) The effect of adding amount of CTAB, (b) concentration of hydrochloric acid, (c) hydrothermal synthesis temperature and (d) hydrothermal synthesis time on the extraction of silica.

Based on these results, the optimal leaching condition was determined to be: particle size of 200 mesh, alkali concentration of 15%, reaction temperature of 95 °C, and reaction time of 120 min, which gave the silica extraction efficiency of 65.30%.

2. Preparation of MS

It has been reported that more highly ordered MS can be formed at higher surface active agent concentrations above the critical micelle concentration (CMC) [34,35]. In the present work, CTAB was used as the surface active agent. We found that the metal ion adsorption capacity of the as-prepared MS increased with the increase of CTAB dose to 0.5 g and remained steady as the CTAB dose further increased to 1.0 g (Fig. 2(a)). The maximum adsorption was measured to be 33.18 mg/g. The SEM imaging suggested that the MS prepared with 0.5 g CTAB contained spherical particles with big spaces between them (Figs. 2(c) and 3). At the low CTAB dose of 0.05 g, the as-synthesized MS tended to aggregate, and the reaction with 1.0 CTAB afforded a yellow solid. Therefore, the CTAB dose was optimized as 0.5 g.

SiO_3^{2-} (Na_2SiO_3) was gradually converted to silica gel with the addition of HCl. Therefore, the effects of HCl concentration on the Cu^{2+} adsorption capacity of the as-prepared MS were investigated in the range of 0.5 to 3.5 mol/L with 0.5 g CTAB at 120 °C. The reaction time was set to 120 min. As shown in Fig. 2(b). The SiO_3^{2-} (Na_2SiO_3) solution reacted with HCl to get silica gel and the specific reaction processes were as follows:

$$Na_2SiO_3=2Na^+ + SiO_3^{2-} \quad (14)$$

$$SiO_3^{2-} + H^+ = HSiO_3^- \quad (15)$$

$$HSiO_3^- + H^+ = H_2SiO_3 \quad (16)$$

$$H_2SiO_3 = H_2O + SiO_2 \quad (17)$$

The formation rate of silica gel increased with the increase of HCl (H^+) concentration, and the precipitation of silica gel burst as the HCl concentration increased to 2.5 mol/L. Further increasing HCl concentration resulted in agglomerations of silica gel with lower porosities, which exhibited lower Cu^{2+} adsorption capacities. Therefore, HCl concentration was set to 2.5 mol/L in the following experiments.

The influence of reaction temperature on the Cu^{2+} adsorption capacity was then studied in the range of 20-150 °C. As shown in Fig. 2(c), the MS prepared at 120 °C showed the highest Cu^{2+} adsorption capacity (37 mg/g). Further analysis suggested that the MS prepared at 120 °C was well dispersed and exhibited a cross-linking structure, which explained its high metal ion adsorption performance. Therefore, the reaction temperature was optimized to be 120 °C.

The morphology of MS was formed before the hydrothermal reaction. Therefore, hydrothermal reaction time could only affect the order and porosity of the MS. The hydrothermal reaction formed the mesoscopic structure of MS, and the degree of order of the mesoscopic structure increased as the reaction time increased. Fig. 2(d) shows the Cu^{2+} adsorption capacities of MS prepared with different hydrothermal reaction times. The Cu^{2+} adsorption capacity increased from 22.05 mg/g to 33.19 mg/g as the reaction time increased from 4 h to 24 h, and further increasing the reaction time decreased the Cu^{2+} adsorption capacity. Based on these results, and

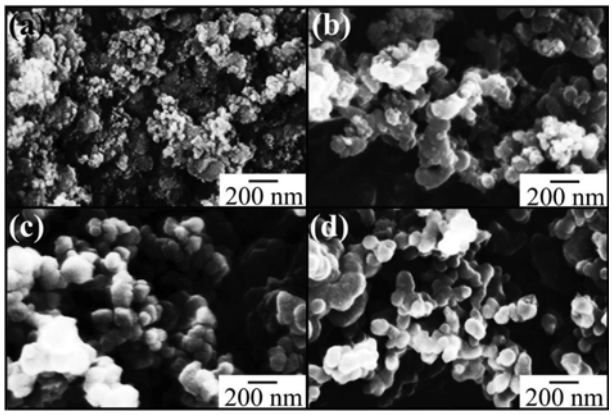

Fig. 3. The effect different CTAB addition on the extraction of silica.

taking the production cost into consideration, the hydrothermal reaction time was optimized to be 24 h.

Fig. 3 shows the SEM images of MS prepared at different CTAB doses. The MS prepared with 0.05 g CTAB were well dispersed particles with irregular shapes and no pore was observed on the particle surface (Fig. 3(a)). The particles of MS prepared with 0.075 g and 1 g CTAB exhibited fewer irregular shapes and few pores on surface, and were partially aggregated (Fig. 3(b) and (c)). No agglomeration was observed in the MS prepared with 0.25 g CTAB and the particle size was measured to be ~238 nm. Therefore, the optimal CTAB dosage was determined to be 0.25 g.

3. Characterization of Synthesized MS under Optimal Conditions

Fig. 4(a) shows the FTIR spectra of MS prepared under optimal conditions. The band at 3,427 cm^{-1} was attributed to the stretching of O-H in the surface silanol and adsorbed water. The band at

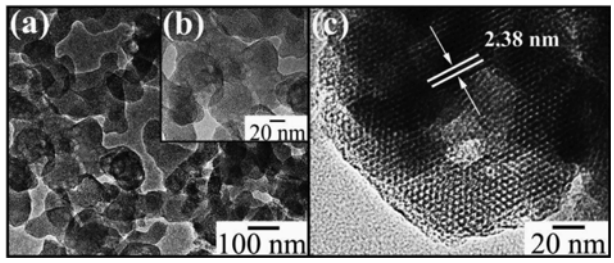

Fig. 5. (a) and (b) are the different amplification districts of the TEM images; (c) is the HRTEM of the final mesoporous silica materials.

1,637 cm^{-1} can be assigned to the deformation mode of adsorbed water [36]. The characteristic peaks at 1,092 and 800 cm^{-1} were due to the anti-symmetric and symmetric stretching vibration of Si-O, respectively [37]. The sharp peak at 470 cm^{-1} was ascribed to the bending vibration of Si-O-Si in the MS [38]. The wide weak XRD bands of the as-prepared MS at 2θ=20-30° (Fig. 4(b)) revealed that it was amorphous, consistent with the results reported in the literature [39]. SEM imaging suggested that the as-prepared MS was regular spherical particles with the size of ~238 nm and the surfaces of most of particles were porous (Fig. 4(c)). The elemental composition of MS was found be to O and Si by EDS analysis (Fig. 4(d)). C and Cu peaks were due to the copper grid. Trace amounts of Al, Mg, and Ga were also detected.

The surface porous structure of MS was then imaged by TEM and HRTEM. The mesopores on some MS samples exhibited uniform pore sizes with ordered hexagonal array distributions (Fig. 5). The distances between the fringes of pores in the mesoporous structure were measured to be ~3 nm. The pores on some samples showed hexagonal distributions of in some key areas, if not

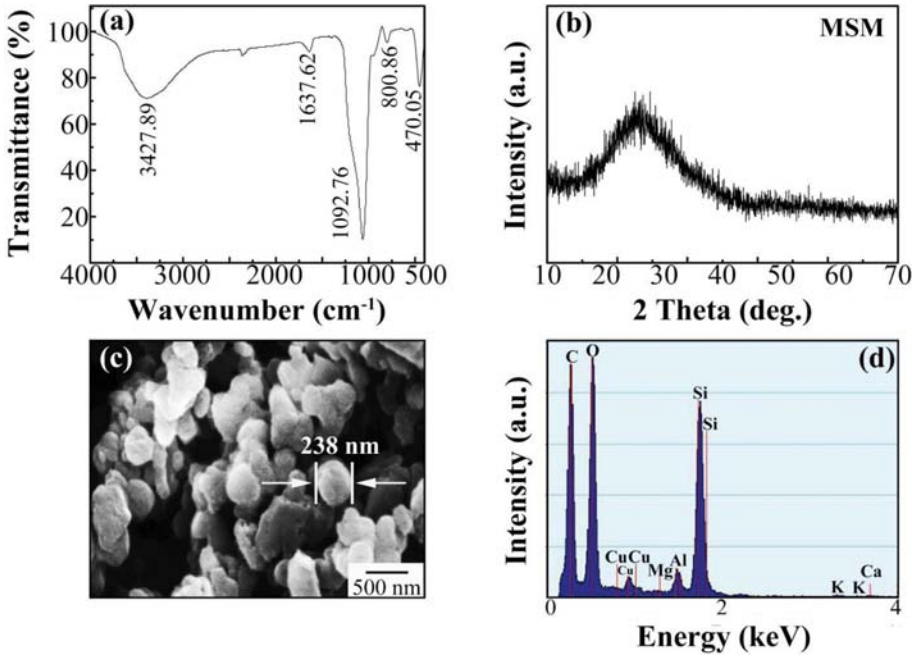

Fig. 4. (a) The FT-IR spectra, (b) XRD, (c) SEM and (d) energy spectrum of the final mesoporous silica materials.

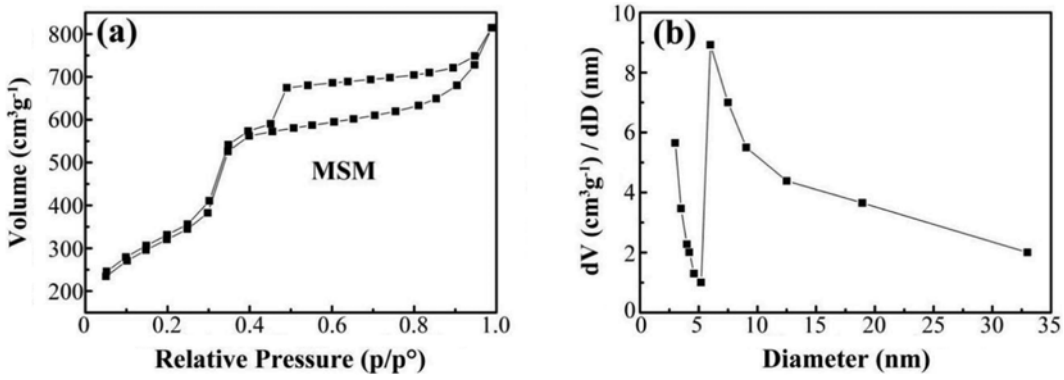

Fig. 6. (a) N_2 adsorption desorption isotherms and (b) pore size distributions of the as-prepared mesoporous silica materials.

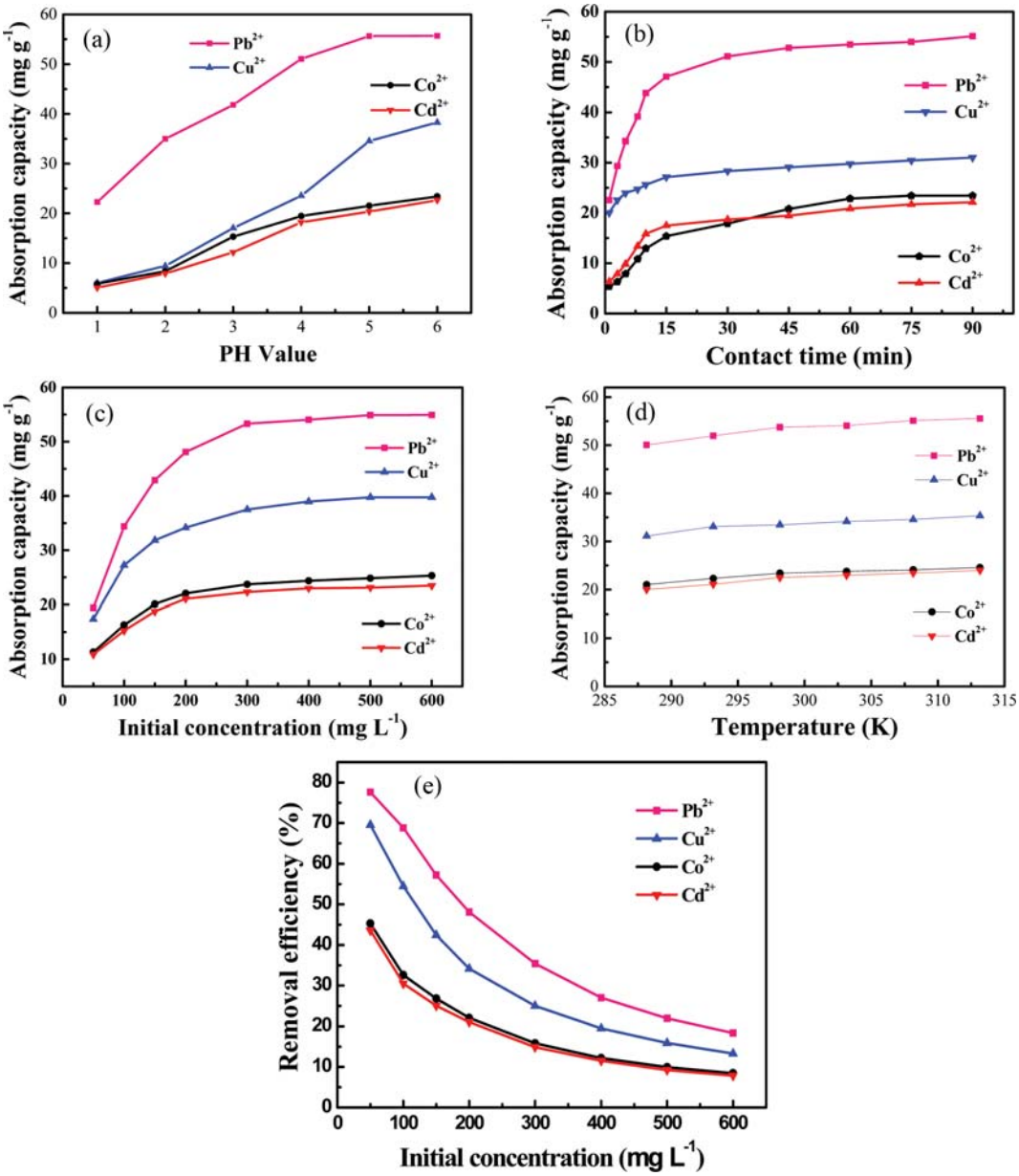

Fig. 7. The effect of pH value (a), contact time (b), initial concentration (c), temperature (d), on the adsorption capacities of Pb^{2+}, Cu^{2+}, Co^{2+} and Cd^{2+} ions. (e) Effect of initial concentration on removal rate.

highly ordered. These results are in good agreement with the results reported in the literature [40-42].

The specific surface area and porosity of the as-prepared MS were also measured. The MS samples exhibited typical type IV isotherm curves (Fig. 6(a)), which confirmed their mesoporous structure. The BET surface area of the as-prepared MS reached 1,199 m^2/g under the optimal conditions. Fig. 6(b) depicts the corresponding pore size distribution and average pore size of 3.43 nm.

4. Metal Ion Adsorption

4-1. Effect of pH

The pH of adsorption solution also exhibited great effects on the metal ion adsorption capacity of the as-prepared MS. Because the metal ions would be converted to the corresponding insoluble hydroxides at pHs over 6, adsorption experiments were conducted in the pH range of 1-6 at 298.15 K with 0.1 g adsorbent for 2 h, and the initial concentrations of metal ions were 200 mg/L. As shown in Fig. 7(a), the uptakes of all metal ions increased with the increase of pH from 1 to 5 and remained stable in the pH range of 5-6. As the reaction progressed with an increase in pH, the electrostatic repulsion force decreased with the increase of pH value, which led to the increase of metal adsorption [43]. It can be explained that the hydrogen ions competed with the metal ions on the same adsorption sites, and the concentration of hydrogen ion decreased with the increase of pH.

4-2. Effect of Contact Time

Contact time is an important parameter affecting the adsorption behavior of an adsorbent. The effects of contact time on the Pb^{2+}, Cu^{2+}, Co^{2+} and Cd^{2+} uptakes of the as-prepared MS were investigated in the range of 1-180 min with 0.1 g adsorbent in 200 mg/mL metal ion solution at 298 K and pH=6. As shown in Fig. 7(b), the uptakes of all metal ions increased dramatically as the contact time increased from 1 min to 90 min; therefore, a 90-min contact time was considered a feasible time for adsorption [44]. And then gradually increased with the increasing of contact time to 120 min and became constant thereafter. In addition, the MS exhibited a burst and linearly increased in metal ion uptake in the first 15 min because of the large number of available adsorption sites that provided high probability for the adsorption. As the available adsorption site gradually decreased and eventually saturated, the adsorption reached the adsorption equilibrium [44].

4-3. Effect of Initial Concentration

Fig. 7(c) shows the effects of initial metal ion concentration on the adsorption behavior of MS. The experiment was conducted at 298.15 K with 0.1 g adsorbent for 120 min. It is clear that all of the metal ion adsorption amounts increased, yet the removal efficiencies decreased with the increasing of initial concentration. At low initial concentrations, the metal ions adsorbed on the MS surface as mono-ionic layers. Multiple adsorption layers were formed only at the high initial concentrations, resulting in high adsorption amounts. However, the number adsorption sites of the MS was limited, which caused the low removal efficiencies for the high concentrations of metal ions.

4-4. Effect of Temperature

The metal ion adsorption capacity was also affected by temperature. Fig. 7(d) shows the metal ion adsorption capacity of MS in the temperature range from 283.15 K to 308.18 K obtained in 120

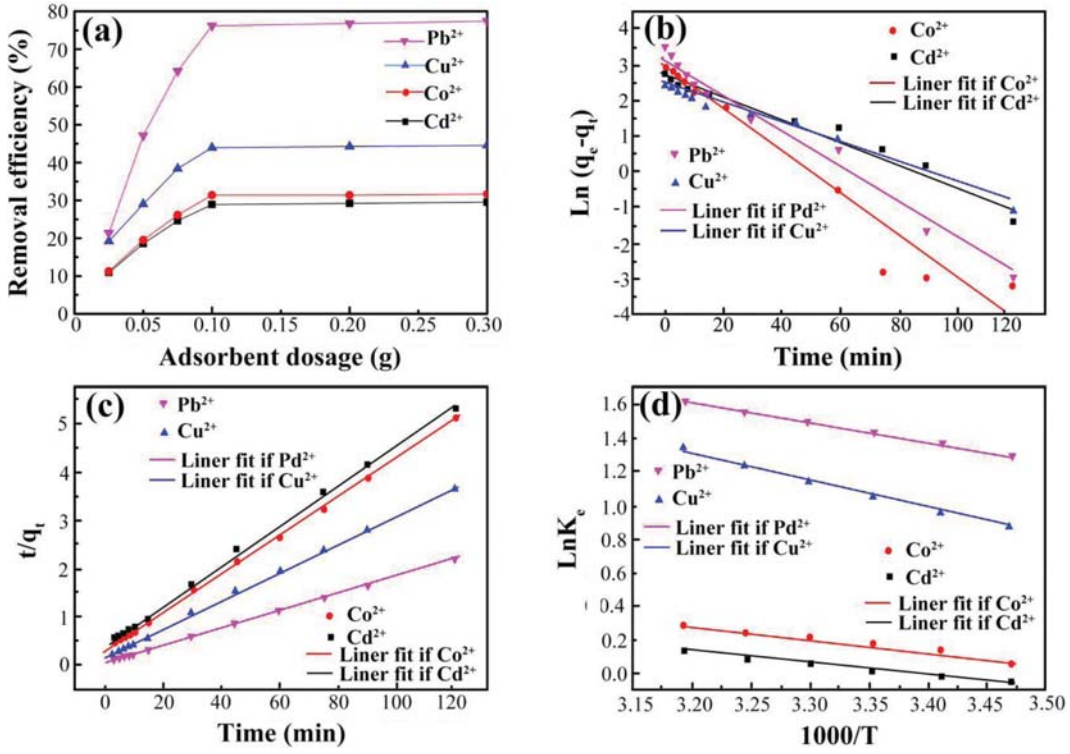

Fig. 8. The effect of the adsorbent dose (a) on the adsorption capacities of Pb^{2+}, Cu^{2+}, Co^{2+} and Cd^{2+} ions. Pseudo-first-order (b) and pseudo-second-order (c) kinetic for the adsorption of Pb^{2+}, Cu^{2+}, Co^{2+} and Cd^{2+} ions. Thermodynamic plots (d) for the adsorption of Pb^{2+}, Cu^{2+}, Co^{2+} and Cd^{2+} ions.

Table 2. Linear fit of pseudo-first-order and pseudo-second-order kinetic models

Metal ions	Q_e(exp) (mg/g)	Pseudo-first-order		Pseudo-second-order	
		10^3k_1 (min^{-1})	R^2	10^3k_2 ($g \cdot mg^{-1} \cdot min^{-1}$)	R^2
Pb^{2+}	55.24	5.06	0.9712	6.07	0.9998
Cu^{2+}	31.87	2.73	0.9789	10.0	0.9976
Co^{2+}	23.4	6.00	0.9336	4.23	0.9958
Cd^{2+}	22.65	3.04	0.9591	5.93	0.9947

Table 3. Adsorption isotherm parameters of the Langmuir isotherms at 288.15 K, 298.15 K, and 308.15 K

Metal ions	Langmuir					
	q_m (mg/g)			R^2		
Temperature	288.15	298.15	308.15	288.15	298.15	308.15
Pb^{2+}	57.97	58.41	58.61	0.9990	0.9994	0.9926
Cu^{2+}	38.05	38.51	38.89	0.9918	0.9952	0.9905
Co^{2+}	26.01	26.94	27.10	0.9945	0.9932	0.9913
Cd^{2+}	24.28	25.11	25.34	0.9813	0.9868	0.9825

min with the initial metal ion concentration of 200 mg/L and 0.1 g of adsorbent at pH=6. It is clear that the metal ion uptake of MS increased with the increase of temperature in the testing range, which showed that metal ion removal was enhanced as the temperature increased [45]. It can be explained that the high temperatures provided sufficient energies for the adsorption. For economic purposes, 298.15 K was chosen in the following experiments.

4-5. Effect of Adsorbent Dose

Fig. 8(a) shows the removal efficiency of the metal ions with different doses of MS in the range of 0.025-0.3 g. The experiments were conducted at the initial metal ion concentration of 200 mg/L at 298.15 K for 120 min. It is clear that higher doses of MS (0.025-0.1 g) removed the metal ions more efficiently, and the removal efficiency gradually became saturated with the increase of MS dose. It can be explained that the surface area and number of adsorption sites increased with the increase of adsorbent dose, yet the removal efficiency remained constant. Therefore, the adsorption capacity gradually decreased with the increase of adsorbent dose due to the decreased available adsorbent sites per unit mass.

5. Kinetic of Adsorption

The metal ion adsorption of MS was then fitted with the pseudo-first-order and second-order kinetic models (Fig. 8(b) and (c)). The pseudo-first-order model assumes that the occupation rate of adsorption sites is proportional to the number of unoccupied sites, and the pseudo-second-order kinetic model considers the adsorption as a chemical reaction where the adsorbate and adsorbent share or exchange electrons. As shown in Table 2, the pseudo-second-order kinetic model fitted the meal ion adsorption on the as-prepared MS well with R^2=0.9997, 0.9976, 0.9958, and 0.9947 for the adsorptions of Pb^{2+}, Cu^{2+}, Co^{2+}, and Cd^{2+}, respectively. In addition, the theoretical Q_e(cal.) values for the Pb^{2+}, Cu^{2+}, Co^{2+} and Cd^{2+} adsorption on the as-prepared MS were calculated to be 56.46 mg/g, 33.28 mg/g, 25.55 mg/g, and 23.23 mg/g, respectively, consistent with the corresponding experimental Q_e(exp.) values. Therefore, the pseudo-second-order kinetic model including the internal diffusion, external diffusion, and surface adsorption can be used to describe the adsorption process accurately. And the pseudo-second-order kinetic model is based on the assumption that the rate limiting step might be chemisorption; it is concluded that the adsorption process using MS is governed by chemisorption [45].

6. Thermodynamic Study

The experimental data were then fitted with Langmuir and Freundlich models, the two most widely used models of adsorption isotherm. Tables 3 and 4 list the fitting results in the temperature range from 288.15 K to 308.15 K. Compared with the Freundlich model, the Langmuir model fitted the experimental data better with a higher R^2 (Tables 3 and 4), and the Langmuir constants (q_m) for the adsorptions of all four ions were in good agreement with the experimental data. These results indicated that the metal ion adsorption on the as-prepared MS was a single layer adsorption, and it means that during the adsorption process monolayer MS covers a homogenous surface and there is no subsequent interaction between adsorbents [46].

Fig. 8(d) and Table 5 show the thermodynamic fitting curves and the calculated thermodynamic parameters, respectively. The positive ΔH suggested that the adsorption was endothermic, and thus

Table 5. Value of thermodynamic parameters for the adsorption of Pb^{2+}, Cu^{2+}, Co^{2+} and Cd^{2+} ions

Metal ions	ΔH (kJ/mol)	ΔS (J/mol K)
Pb^{2+}	9.79	44.46
Cu^{2+}	13.98	55.69
Co^{2+}	6.32	22.53
Cd^{2+}	5.64	19.05

Table 4. Adsorption isotherm parameters of the Freundlich isotherms at 288.15 K, 298.15 K, and 308.15 K

Metal ions	Freundlich								
	k_f			n			R^2		
Temperature	288.15	298.15	308.15	288.15	298.15	308.15	288.15	298.15	308.15
Pb^{2+}	19.54	20.94	22.72	5.51	3.92	6.19	0.8908	0.8471	0.9096
Cu^{2+}	16.96	17.79	18.27	7.18	7.48	7.72	0.9026	0.9045	0.8954
Co^{2+}	4.61	5.4	5.56	3.22	3.87	4.13	0.8990	0.8994	0.9002
Cd^{2+}	4.57	5.21	5.21	3.48	3.96	4.31	0.9019	0.8909	0.9123

n-heterogeneity factor, k_f-Freundlich equilibrium constant

Table 6. Comparison of adsorption capacity of heavy metal ions with other adsorbents

Name of adsorbent	Pb^{2+} (mg/g)	Cu^{2+} (mg/g)	Co^{2+} (mg/g)	Cd^{2+} (mg/g)	Ref.
Chitosan/SiO_2/Fe_3O_4	9.32	31.7	-	4.48	[40]
Sugarcane bagasse	21.28	3.65	-	-	[41]
Cotton fiber	21.62	6.12	-	8.22	[42]
Zeolite-Y	7.91	4.95	-	-	[48]
Polymer Beads. I.	15.33	-	-	12.59	[49]
Polymeric membranes	122.25	29.87	-	37.10	[50]
Polyvinyl alcohol PVA/chitosan magnetic composite	-	-	14.39	-	[47]
GO-Polydopamine	53.6	24.4		33.3	[46]
MS	55.24	33.01	23.4	22.65	This work

the adsorption capacity increased with the increase of temperature [47]. The positive entropy change suggests that the adsorption process was enthalpy driven.

Table 6 lists the adsorption capacities of the as-prepared for the metal ions mentioned above under optimal conditions. Table 6 shows that the synthesized MS has good adsorption performance for heavy metal ions. It has important environmental and economic benefits for realizing high value utilization of coal slag resources.

CONCLUSIONS

A mesoporous silica was successfully prepared from coal slag via alkaline leaching and hydrothermal reaction. The SiO_3^{2-} leaching liquid was obtained by leaching coal slag with an NaOH aqueous solution at 95 °C for 2 h under stirring at 300 rpm. The sodium silicate was precipitated in 0.05 g/mL CTAB at 40 °C by gradually adding 2.5 mol/L HCl until pH was adjusted to 10. The mixture was heated at 120 °C in a hydrothermal synthesis reactor for 24 h. The crude product was filtered, washed, dried for 12 h in air, and calcined at 550 °C for 6 h at a heating rate of 2 °C/min to afford the desired MS. The metal ion adsorption behavior of the as-prepared MS was found to follow the pseudo-second-order kinetics, and thus was a chemical adsorption. The adsorption isotherm fitted the Langmuir model, suggest that the metal ion adsorption on the as-prepared MS was a single layer adsorption. Our work has provided a new strategy for the utilization of coal slag and an economic way for metal ion removal.

ACKNOWLEDGEMENTS

This work was supported by the National Natural Science Foundation of China (Project No. 21466028), the Inner Mongolia Science and Technology Key Projects, the Program for Grassland Excellent Talents of Inner Mongolia Autonomous Region, and training plan of academic backbone in youth of Inner Mongolia University of Technology.

REFERENCES

1. C. Li, J. Wan, H. Sun and L. Li, *J. Hazard. Mater.*, **179**, 515 (2010).
2. A. Kondratiev and A. Ilyushechkin, *Fuel*, **224**, 783 (2018).
3. H. Tanaka, Y. Sakai and R. Hino, *Mater. Res. Bull.*, **37**, 1873 (2002).
4. M. Nisnevich, G. Sirotin, T. Schlesinger and Y. A. Eshel, *Fuel*, **87**(8), 1610 (2008).
5. M. Park, C. L. Choi, W. T. Lim, M. C. Kim, J. Choi and N. H. Heo, *Micropor. Mesopor. Mater.*, **37**, 81 (2000).
6. C. Zevenbergen, J. P. Bradley, L. P. V. Reeuwijk, A. K. Shyam, O. Hjelmar and R. N. J. Comans, *Environ. Sci. Technol.*, **33**(19), 3405 (1999).
7. Y. Li, Y. Liu, X. Z. Gong, Z. R. Nie, S. P. Cui, Z. H. Wang and W. J. Chen, *J. Clean. Prod.*, **120**(175), 221 (2016).
8. D. A. Pan, L. L. Li, Y. F. Wu, T. T. Liu and H. L. Yu, *J. Clean. Prod.*, **175**, 251 (2018).
9. P. Torkittikul, T. Nochaiya, W. Wongkeo and A. Chaipanich, *J. Mater. Cycles. Waste*, **19**(1), 305 (2017).
10. N. Rivera, D. Hesterberg, N. O. Kaur and W. Duckworth, *Energy Fuel*, **31**(9), 9652 (2017).
11. K. Hui and C. Chao, *Micropor. Mesopor. Mater.*, **88**, 145 (2006).
12. F. Yan, J. G. Jiang, S. C. Tian, Z. W. Liu, J. Shi, K. M. Li, X. J. Chen and Y. W. Xiu, *ACS Sustain. Chem. Eng.*, **4**(9), 4654 (2016).
13. D. P. Serrano, R. V. Grieken, A. M. Melgares and J. Moreno, *J. Am. Chem. Soc.*, **17**(4), 387 (2010).
14. H. T. Liu, X. J. Bao, W. S. Wei and G. Shi, *Micropor. Mesopor. Mater.*, **66**(1), 117 (2003).
15. R. Y. Zhang, W. Ding, B. Tu and D. Y. Zhao, *Chem. Mater.*, **19**, 4379 (2007).
16. M. Kruk, M. Jaronic and A. Sayari, *J. Phys. Chem. B*, **101**, 583 (1997).
17. P. V. D. Voort, M. F. Mathieu, A. Mees and E. F. Vansant, *J. Phys. Chem. B*, **102**(44), 8847 (1998).
18. H. J. Lee, K. K. Park, M. Kupnik, N. A. Melosh and B. T. Khuriyakub, *Anal. Chem.*, **84**(7), 3063 (2012).
19. D. H. Zhang, D. Y. Xiao, Q. Yu, S. F. Chen and M. H. Miao, *ACS Sustain. Chem. Eng.*, **5**(11), 10258 (2017).
20. A. Nakamizu, T. Kasai, J. Nakazawa and S. Hikichi, *ACS Omega*, **2**(3), 1025 (2017).
21. S. J. Huang, C. T. Hung, A. M. Zheng, J. S. Lin, C. F. Yang, Y. C. Chang, F. Deng and S. B. Liu, *J. Phys. Chem. Lett.*, **5**, 3183 (2014).
22. M. J. Climent, A. Corma, G. R. Lopez, S. Iborra and J. Primo, *J. Catal.*, **161**(2), 783 (1996).
23. D. Clifford, S. Subramonian and T. J. Sorg, *Environ. Sci. Technol.*, **20**(11), 1072 (1986).
24. S. Babel and T. A. Kurniawan, *J. Hazard. Mater.*, **97**(1), 219 (2003).
25. C. Hui, Y. H. Chao and S. C. Kot, *J. Hazard. Mater.*, **127**(1), 89 (2005).
26. A. Sayari, S. Hamoudi and Y. Yang, *Chem. Mater.*, **17**(1), 212 (2005).

27. J. P. Ruparelia, S. P. Duttagupta, A. K. Chatterjee and S. Mukherji, *Desalination*, **232**(1), 145 (2008).
28. S. H. Lin and R. S. Juang, *J. Hazard. Mater.*, **92**, 315 (2002).
29. Y. S. Ho and A. E. Ofomaja, *J. Hazard. Mater.*, **129**(1), 137 (2006).
30. L. Martinson, M. Alveteg and P. Warfvinge *Environ. Pollut.*, **124**(1), 119 (2003).
31. Q. Gao, H. Li, Y. Ling, B. Han, K. Xia and C. Zhou, *Micropor. Mesopor. Mater.*, **241**, 409 (2017).
32. M. Prasad, S. Saxena, S. S. Amritphale and N. Chandra, *Ind. Eng. Chem. Res.*, **39**(8), 3034 (2000).
33. D. H. Ding, Z. F. Lei, Y. N. Yang, C. P. Feng and Z. Y. Zhang, *ACS Appl. Mater. Interfaces*, **5**(20), 10151 (2013).
34. K. Kageyama, J. Tamazawa and T. Aida, *Science*, **285**, 2113 (1999).
35. H. Takahashi, B. Li, T. Sasaki, C. Miyazaki, T. Kajino and S. Inagaki, *Chem. Mater.*, **12**, 3301 (2000).
36. G. J. Yuan, J. B. Zhang, Y. F. Zhang, Y. Yan, X. Ju and J. Sun, *Korean J. Chem. Eng.*, **32**(3), 436 (2015).
37. A. A. Romero, M. D. Alba, W. Z. Zhou and J. Klinowski, *J. Phys. Chem. B*, **101**, 5294 (1997).
38. R. Takahashi, S. Sato, T. Sodesawa, M. K. Kawakita and J. Ogura, *J. Phys. Chem. B*, **104**, 12184 (2000).
39. T. Jesionowski, *Powder Technol.*, **127**(1), 56 (2002).
40. S. Venkateswarlu, B. N. Kumar, B. Prathima, Y. SubbaRao and N. V. V. Jyothi, *Arabian J. Chem.*, **7**, 1878 (2014).
41. W. P. Putra, A. Kamari, S. N. M. Yusoff, C. F. Ishak, A. Mohamed, N. Hashim and I. M. Isa, *J. Encapsulation Adsorpt. Sci.*, **4**, 25 (2014).
42. Á. G. Paulino, A. J. D. Cunha, R. V. D. S. Alfaya and A. A. D. S. Alfaya, *Water Treat.*, **52**, 4223 (2014).
43. K. Kamel, A. Zboon, M. Bashar, A. Smadi and A. Khawaldh, *Water, Air, & Soil Pollution*, **227**, 248 (2016).
44. A. Kamel, A. Mohammad and F. B. Hani, *J. Hazard. Mater.*, **188**, 414 (2011).
45. S. Mohammad, A. Harahsheh, A. Z. Kamel and A. M. Leema, *Chem. Eng. J.*, **3**, 1669 (2015).
46. Z. Dong, D. Wang, X. Liu, X. F. Pei, L. W. Chen and J. Jin, *J. Mater. Chem. A*, **2**, 5034 (2014).
47. Y. Zhu, J. Hu and J. Wang, *Prog. Nucl. Energy*, **71**, 172 (2014).
48. L. C. Lin, M. Thirumavalavan, Y. T. Wang and J. F. Lee, *Colloids Surf., A: Physicochem. Eng. Aspects*, **369**, 223 (2010).
49. G. N. Moroi, E. Avram and L. Bulgariu, *Water, Air, & Soil Pollution*, **227**, 260 (2016).
50. H. Bessbousse, T. Rhlalou, J. F. Verchere and L. Lebrun, *J. Membr. Sci.*, **307**, 249 (2008).